universe

MDPI

Article

Simultaneous Analysis of Midrapidity p_T Spectra of Identified Particle Species in Pb + Pb Collisions at $\sqrt{s_{nn}}$ = 2.76 TeV Using Tsallis Distribution with Transverse Flow

Khusniddin K. Olimov [1,2,*], Igor A. Lebedev [3], Anastasiya I. Fedosimova [3,4], Fu-Hu Liu [5], Shakhnoza Z. Kanokova [1], Maratbek Z. Shodmonov [1] and Boburbek J. Tukhtaev [1]

1 Physical-Technical Institute of Uzbekistan Academy of Sciences, Chingiz Aytmatov Str. 2b, Tashkent 100084, Uzbekistan
2 Faculty of Engineering, New Uzbekistan University (NUU), Tashkent 100007, Uzbekistan
3 Institute of Physics and Technology, Satbayev University, Almaty 050032, Kazakhstan
4 Institute of Nuclear Physics, Almaty 050032, Kazakhstan
5 Institute of Theoretical Physics, Collaborative Innovation Center of Extreme Optics, State Key Laboratory of Quantum Optics and Quantum Optics Devices, Shanxi University, Taiyuan 030006, China
* Correspondence: khkolimov@gmail.com or kh.olimov@uzsci.net

Abstract: The midrapidity transverse momentum distributions of the charged pions, kaons, protons, and antiprotons in ten groups of centrality of Pb + Pb collisions at $\sqrt{s_{nn}}$ = 2.76 TeV, measured by the ALICE Collaboration, have been analyzed successfully using both thermodynamically consistent and non-consistent Tsallis distribution functions with transverse flow. The collision centrality dependencies of the extracted parameters of two kinds of Tsallis functions with transverse flow have been investigated. The significantly different behavior (growth rates) of $\langle\beta_T\rangle$ in regions $\langle N_{part}\rangle < 71$ and $\langle N_{part}\rangle > 71$ with the temperature T_0 becoming constant in region $\langle N_{part}\rangle > 71$ has been observed. This could indicate that $\langle N_{part}\rangle = 71 \pm 5$ (corresponding to $\langle dN_{ch}/d\eta\rangle = 205 \pm 15$) is a threshold border value of collision centrality for crossover phase transition from the dense hadronic state to the QGP state (or a mixed state of QGP and hadrons) in Pb + Pb collisions at $\sqrt{s_{nn}}$ = 2.76 TeV. This conjecture is supported further by the observed, significantly different correlations between T_0 and $\langle\beta_T\rangle$ parameters in the corresponding $\langle\beta_T\rangle < 0.44$ and $\langle\beta_T\rangle > 0.44$ ranges. The strong positive linear correlation between non-extensivity parameter q for pions and kaons, between q for pions and (anti)protons, and between q for kaons and (anti)protons has been obtained. The parameter q for all studied particle species has proven to be strongly anticorrelated with the average transverse flow velocity, $\langle\beta_T\rangle$. Quite a large positive linear correlation has been obtained between the q of the studied particle species and temperature parameter T_0. Analysis of q versus $\langle N_{part}\rangle$ dependencies for the studied particle species suggests that the highly thermalized and equilibrated QGP is produced in central Pb + Pb collisions at $\sqrt{s_{nn}}$ = 2.76 TeV with $\langle N_{part}\rangle > 160$.

Keywords: Pb + Pb collisions at the LHC; transverse momentum distributions; Tsallis statistics with transverse flow; system thermalization and equilibrium; phase transition to QGP; non-extensivity parameter q

check for updates

Citation: Olimov, K.K.; Lebedev, I.A.; Fedosimova, A.I.; Liu, F.-H.; Kanokova, S.Z.; Shodmonov, M.Z.; Tukhtaev, B.J. Simultaneous Analysis of Midrapidity p_T Spectra of Identified Particle Species in Pb + Pb Collisions at $\sqrt{s_{nn}}$ = 2.76 TeV Using Tsallis Distribution with Transverse Flow. *Universe* **2022**, *8*, 655. https://doi.org/10.3390/universe8120655

Academic Editor: Maxim Chernodub

Received: 4 November 2022
Accepted: 10 December 2022
Published: 13 December 2022

Publisher's Note: MDPI stays neutral with regard to jurisdictional claims in published maps and institutional affiliations.

1. Introduction

There is great importance and interest in investigating the properties of the short-lived and deconfined state of almost-free quarks and gluons, called quark–gluon plasma (QGP), which can be produced in high-energy nucleus–nucleus collisions. It is believed that the universe was in a state of QGP a few microseconds after the so-called Big Bang, considered to be the starting point in the birth of our universe. The striking evidence about the creation of QGP in high-energy heavy-ion collisions was reported in early works seen in Refs. [1–9]. It was found that the produced QGP was characterized by a fluid-like

behavior with low viscosity. The modern experiments on high-energy heavy ions as well as proton–proton collisions at the RHIC (Relativistic heavy-ion collider, Brookhaven National Laboratory (BNL), Upton, NY, USA) and LHC (Large hadron collider, CERN, Switzerland) produce and measure tens of millions of collisions for the large HEP (high energy physics) community of scientists from around the world to analyze, and reveal various collective properties of the hot and dense matter, which has a very short lifetime of the order of 10^{-23} s. Naturally, the properties of the created QGP and swiftly expanding matter found afterwards are deduced from the analysis of the kinematical characteristics of the final particles reaching the detectors with the help of the theoretical and phenomenological approaches, including those based on thermal and hydrodynamic models, and various models of extensive and non-extensive statistics. The hot and dense matter swiftly expands right after QGP's creation, and it passes through the subsequent chemical and kinetic freeze-out stages, which fix the content of particle species and the final momenta of these particles, respectively. The large statistics, expressed by the huge number of particles produced in high-energy heavy-ion, and proton–proton collisions in the modern collider experiments, justifies the use of various statistical models and approaches for the HEP data analysis.

The chemical freeze-out parameters, such as the temperature $T_{\rm ch}$ and the baryochemical potential $\mu_{\rm b}$ at the moment of chemical freeze-out are extracted by performing fits of the particle abundancies and their ratios with the thermal, statistical hadronization models [10–15]. The kinetic freeze-out parameters, such as the transverse flow velocity and the corresponding temperature at the moment of kinetic freeze-out, are obtained [10,16–33] from fitting the transverse momentum (p_T) distributions of particles with the help of various theoretical and phenomenological model functions, including the hydro-inspired blast-wave models.

The non-extensive statistical distributions, particularly various forms of non-extensive Tsallis distribution functions, have been widely used to describe the p_T distributions of particles in high-energy collisions [34–48]. Different kinds of Tsallis functions were extremely successful in describing the p_T spectra of particles in high-energy proton–proton collisions up to the highest p_T values measured at the RHIC and LHC experiments. The advantage of using the Tsallis distribution function is in its connection, via entropy, to thermodynamics [43], which is not the case with many other power law distributions. The important parameters of the Tsallis distribution function are the effective temperature (T) and the non-extensivity parameter q, which measures the degree of deviation of p_T distribution from the exponential Boltzmann–Gibbs distribution. The q parameter is also said to characterize the degree of non-thermalization or non-equilibrium of the system [47]. Furthermore, the parameters q and T of the Tsallis function can be employed to identify the system size scaling and initial conditions [49]. Due to the effective temperature containing the contribution of both the chaotic thermal motion and transverse radial flow, the transverse flow should be embedded into the Tsallis distribution function in order to disentangle these two effects. For the description of the p_T spectra of particles in high-energy heavy-ion collisions, different transverse expansion models are embedded into Tsallis statistics. To extract the kinetic freeze-out temperature and transverse flow velocity, different model functions have been used [10,16–33]: the Blast-Wave model with Boltzmann–Gibbs statistics (the BGBW model), the Blast-Wave model with Tsallis statistics (the TBW model), the improved Tsallis distribution with flow effect, Hagedorn formula with the embedded transverse flow, and recently [18,33], the Tsallis distribution function with included transverse flow.

The majority of works devoted to the analysis of p_T spectra of particles produced in high-energy collisions with the help of various theoretical model functions, including Tsallis function and its modified forms, have separately fitted the p_T distribution of each particle type in a given collision. As mentioned in Refs. [16,19,22,28,29], it is not possible to extract the collective properties of a system, such as kinetic freeze-out temperature or transverse flow velocity, from separate fits to the p_T spectrum of each particle type. Only the theoretical model fits applied simultaneously to p_T spectra of different particle species by assigning,

for example, the transverse flow velocity and temperature as the common (global) fitted parameters for all particle types can yield the meaningful physical parameters of the studied collision system [16,19,22,28,29]. The collective parameters of the systems produced in high-energy collisions have been extracted and analyzed successfully by applying simultaneous (combined) model fits with just few parameters in Refs. [10,16–19,22,27–29,48].

This study continues from our recent papers [17–19,33] devoted to analysis, applying simultaneous theoretical model fits, of the centrality dependencies of transverse momentum spectra of the charged pions, kaons, protons, and antiprotons produced in high-energy proton–proton, Xe + Xe, and Pb + Pb collisions at the LHC, measured by ALICE Collaboration. Since the pions, kaons, and (anti)protons represent the largest predominant part of the final particles coming from high-energy proton–proton and heavy-ion collisions, we believe that the simultaneous analysis of these particle species can reveal the collective properties of the system produced in these collisions. In Refs. [17,19] we investigated the dependencies of midrapidity p_T spectra of the charged pions, kaons, protons, and antiprotons on charged-particle multiplicity density ($<dN_{ch}/d\eta>$) in proton–proton collisions at $\sqrt{s}$ = 7 and 13 TeV, respectively. The combined minimum χ^2 fits with the thermodynamically consistent Tsallis function and Hagedorn function with transverse flow could quite well reproduce the p_T distributions of the particle species in the analyzed groups of $<dN_{ch}/d\eta>$ in proton–proton collisions at $\sqrt{s}$ = 7 and 13 TeV [17,19]. From the analysis of the $<dN_{ch}/d\eta>$ dependencies of the extracted kinetic freeze-out temperature, T_0, and average transverse flow velocity, $\langle\beta_T\rangle$, it was estimated that the probable onset of the deconfinement phase transition in proton–proton collisions at $\sqrt{s}$ = 7 and 13 TeV occurs at $<dN_{ch}/d\eta> \approx 6.1 \pm 0.3$ [17] and $<dN_{ch}/d\eta> \approx 7.1 \pm 0.2$ [19], respectively. These estimates proved to be consistent with the calculations of Campanini in Refs. [50–52], made using a completely different method for high-energy proton–proton collisions, and theoretical predictions [52] in case of crossover transition from hadronic gas to the QGP phase starting at $(dN_{ch}/d\eta) \approx 6$. The $<dN_{ch}/d\eta>$ dependence of the effective temperature T of the Tsallis function with thermodynamical consistence in proton–proton collisions at both $\sqrt{s}$ = 7 and 13 TeV was described quite well by the simple power function, $T \sim< \frac{dN_{ch}}{d\eta} >^{1/3}$, with the same ($\approx$1/3) exponent parameter [17,19].

In Refs. [18,33] we studied the dependencies of midrapidity p_T spectra of the charged pions, kaons, protons, and antiprotons, measured by ALICE Collaboration, on the average number of participant nucleons, $\langle N_{part}\rangle$, in Xe+Xe collisions at $\sqrt{s_{nn}}$ = 5.44 TeV and Pb + Pb collisions at $\sqrt{s_{nn}}$ = 5.02 TeV, respectively. The combined minimum χ^2 fits with thermodynamically consistent and non-consistent Tsallis function with embedded transverse flow could describe quite well the p_T distributions of the studied particle species in various collision centralities, defined by $\langle N_{part}\rangle$, in Xe + Xe and Pb + Pb collisions at $\sqrt{s_{nn}}$ = 5.44 TeV and 5.02 TeV, respectively. From the analysis of the $\langle N_{part}\rangle$ dependencies of the extracted kinetic freeze-out temperature, T_0, and average transverse flow velocity, $\langle\beta_T\rangle$, it was deduced that $\langle N_{part}\rangle \approx 44 \pm 5$ [18] and $\langle N_{part}\rangle \approx 71 \pm 7$ [33] could be the threshold border values of collision centrality for a crossover transition from a dense hadronic state to the QGP phase (or mixed phase of QGP and hadrons) in Xe + Xe and Pb + Pb collisions at $\sqrt{s_{nn}}$ = 5.44 TeV and 5.02 TeV, respectively.

The present work is devoted to the analysis of midrapidity transverse momentum spectra of the charged pions, kaons, protons, and antiprotons at various centralities of Pb + Pb collisions at $\sqrt{s_{nn}}$ = 2.76 TeV, measured by ALICE Collaboration [16]. We will implement the simultaneous minimum χ^2 model fits of the experimental midrapidity p_t distributions of the analyzed particle species in Pb + Pb collisions at $\sqrt{s_{nn}}$ = 2.76 TeV, using thermodynamically consistent as well as non-consistent Tsallis distribution functions with embedded transverse flow, as it was performed in our recent works [18,33] to analyze the midrapidity p_T spectra of the same particle species in Xe + Xe and Pb + Pb collisions at $\sqrt{s_{nn}}$ = 5.44 TeV and 5.02 TeV, respectively. This will allow us to directly compare these three collision systems in order to find new regularities in the collision centrality and energy dependencies of the extracted system parameters.

2. The Data and Models

In this paper, we analyze the transverse momentum distributions of the charged pions, kaons, protons, and antiprotons produced at midrapidity ($|y| < 0.5$) at 10 centrality intervals in Pb + Pb collisions at $\sqrt{s_{nn}}$ = 2.76 TeV, measured by ALICE Collaboration and presented in Ref. [16]. The p_T ranges measured by ALICE Collaboration have been as follows: [0.1–3.0] GeV/c for $\pi^+ + \pi^-$, [0.2–3.0] GeV/c for $K^+ + K^-$, and [0.3–4.6] GeV/c for $p + \overline{p}$. The averages of the number of participant nucleons ($\langle N_{part} \rangle$) and charged-particle (pseudo-rapidity) multiplicity density ($\langle dN_{ch}/d\eta \rangle$) calculated [16,53] using the Glauber–Monte Carlo model in the analyzed ten centrality groups of Pb + Pb collisions at $\sqrt{s_{nn}}$ = 2.76 TeV are shown in Table 1.

Table 1. The average number of participant nucleons and mean charged-particle multiplicity densities [16,53] in the analyzed groups of centralities of Pb + Pb collisions at $\sqrt{s_{nn}}$ = 2.76 TeV.

Centr.	$\langle N_{part} \rangle$	$\langle dN_{ch}/d\eta \rangle$
0–5%	382 ± 14	1601 ± 60
5–10%	328 ± 13	1294 ± 49
10–20%	260 ± 10	966 ± 37
20–30%	187 ± 7	649 ± 23
30–40%	130 ± 5	426 ± 15
40–50%	87 ± 3	261 ± 9
50–60%	54 ± 2	149 ± 6
60–70%	31 ± 2	76 ± 4
70–80%	16 ± 2	35 ± 2
80–90%	7 ± 1	13 ± 2

There are several modifications [27,38,39,43–46,54,55] of the Tsallis distribution function, which provide comparably equal quality of fits of p_T distributions of particles produced in high-energy collisions. One of the simple variants [45] of Tsallis function is represented at midrapidity (mid-y) ($<y> = 0$) as:

$$\frac{d^2N}{2\pi N_{ev} p_T dp_T dy} = C\left(1 + (q-1)\frac{m_T}{T}\right)^{-\frac{q}{q-1}}, \quad (1)$$

where C is the normalization constant, N_{ev}—is the total number of the inelastic events, $m_T = \sqrt{p_T^2 + m_0^2}$ is the transverse mass (energy), and m_0—the rest mass of a hadron. The parameter T is the effective temperature, and q is the non-extensivity parameter. We call this function in Equation (1) the thermodynamically non-consistent Tsallis distribution or simple (non-consistent) Tsallis function in the present work. The q is an important parameter, which accounts for the deviation of the p_T distribution from the exponential Boltzmann–Gibbs distribution. At the limit $q \to 1$, the Tsallis function reduces to the exponential, or equilibrated, Boltzmann–Gibbs distribution. The closer the parameter q is to one (1), the more equilibrated and thermalized the system is.

The following version [38,43–45] of the Tsallis distribution derived at zero chemical potential (μ is approximately zero at the highest (TeV range) collision energies at the LHC) at mid-y satisfies the thermodynamical expressions for the particle number, temperature, pressure, entropy, and energy densities:

$$\frac{d^2N}{2\pi N_{ev} p_T dp_T dy} = C_q m_T \left(1 + (q-1)\frac{m_T}{T}\right)^{-q/(q-1)}, \quad (2)$$

which we call a Tsallis function with thermodynamical consistence or (thermodynamically) consistent Tsallis function (distribution) in the present work. In Ref. [38] the proof of the thermodynamical consistence of the function in Equation (2) was presented. The fitting constant, C_q, is thought to be related linearly to the volume (V) of the system [38,43] via the

relation $C_q = gV/(2\pi)^3$, with g denoting the degeneracy factor. The degeneracy factor g is equal to two, three, or four for protons, pions, and kaons, respectively.

The effective temperature parameter T in Equations (1) and (2) contains the contribution of both the chaotic thermal motion and transverse flow. As already mentioned, the transverse flow velocity is incorporated into the Tsallis function in order to disentangle these two effects.

In Refs. [17,19,27–29,48] the transverse expansion velocity has been embedded into a QCD-inspired Hagedorn function, $\frac{d^2N}{2\pi N_{ev} p_T dp_T dy} = C_n \left(1 + \frac{m_T}{p_0}\right)^{-n}$, by substituting $p_0 = nT_0$ and implementing the Lorentz transformation $m_T \rightarrow \langle\gamma_T\rangle(m_T - p_T\langle\beta_T\rangle)$ to arrive, finally, at the Hagedorn function with (embedded) transverse flow:

$$\frac{d^2N}{2\pi N_{ev} p_T dp_T dy} = C_n \left(1 + \langle\gamma_T\rangle \frac{(m_T - p_T\langle\beta_T\rangle)}{nT_0}\right)^{-n}. \quad (3)$$

Here, C_n is the normalization constant, $\langle\gamma_T\rangle = 1/\sqrt{1 - \langle\beta_T\rangle^2}$, and $\langle\beta_T\rangle$ is the average transverse flow velocity; T_0 estimates the kinetic freeze-out temperature, and n is the free parameter. The substitution $m_T \rightarrow \langle\gamma_T\rangle(m_T - p_T\langle\beta_T\rangle)$, applied to derive Equation (3), denotes simply the Lorentz transformation to a system co-moving with the average flow velocity, $\langle\beta_T\rangle$, of particles in the transverse plane assuming the existence of such a flow of particles in this co-moving frame [27]. The p_T distributions of particles in proton+proton and heavy-ion collisions at the RHIC and LHC were reproduced quite well [17,19,27–29,48] by the combined fits with the Hagedorn function with transverse flow (Equation (3)), and the extracted parameters could be interpreted physically.

To describe midrapidity p_T distributions of identified charged particles in various centralities of Pb + Pb collisions at $\sqrt{s_{nn}}$ = 2.76 TeV in the present work, we incorporate the transverse flow velocity into the Tsallis function in Equation (1) by implementing, as was performed for the first time in Ref. [18], the Lorentz transformation $m_T \rightarrow \langle\gamma_T\rangle(m_T - p_T\langle\beta_T\rangle)$:

$$\frac{d^2N}{2\pi N_{ev} p_T dp_T dy} = C \left(1 + \langle\gamma_T\rangle \frac{(q-1)(m_T - p_T\langle\beta_T\rangle)}{T_0}\right)^{-q/(q-1)}, \quad (4)$$

which we call the non-consistent or simple Tsallis function with transverse flow in present analysis.

Similarly, we embed the transverse flow into Tsallis distribution with thermodynamical consistence in Equation (2) by substituting $m_T \rightarrow \langle\gamma_T\rangle(m_T - p_T\langle\beta_T\rangle)$ to obtain [18] the function

$$\frac{d^2N}{2\pi N_{ev} p_T dp_T dy} = C_q \langle\gamma_T\rangle(m_T - p_T\langle\beta_T\rangle)\left(1 + \langle\gamma_T\rangle \frac{(q-1)(m_T - p_T\langle\beta_T\rangle)}{T_0}\right)^{-q/(q-1)}, \quad (5)$$

which we call a thermodynamically consistent or consistent Tsallis function with transverse flow in present analysis.

The combined (simultaneous) fits by the model functions in Equations (4) and (5) of midrapidity p_T distributions of the analyzed particle species in each centrality group have been performed with the help of Nonlinear Curve Fitting of the Origin 9.1 Graphing and Data Analysis Software. During the combined fitting procedures, the parameters T_0 and $\langle\beta_T\rangle$ have been the common (shared) system parameters for the analyzed particle species. The error bars of the experimental data points, shown in the figures, represent the combined statistical and systematic errors (added in quadrature). These combined errors are mostly defined by the systematic ones with negligible statistical uncertainties. The details on the calculation of the systematic errors are given in Ref. [16]. The combined errors have been used to define the weights $(1/(\text{error})^2)$ of the data points during the minimum χ^2 fitting procedures. The p_T intervals measured by ALICE Collaboration in Pb + Pb collisions at $\sqrt{s_{nn}}$ = 2.76 TeV are [16]: [0.1–3.0] GeV/c for $\pi^+ + \pi^-$, [0.2–3.0] GeV/c for $K^+ + K^-$, and

[0.3–4.6] GeV/c for $p + \overline{p}$. The region $p_T < 0.5$ GeV/c in pion spectra is excluded from the fitting procedures, as done previously in Refs. [16–19,22,28,29,33,48], due to the significant contribution to pion production from the decays of baryon resonances in this range. Hence, in the present work we use the following p_T intervals for combined minimum χ^2 fits with the model functions in Equations (4) and (5): [0.5–3.0] GeV/c for $\pi^+ + \pi^-$, [0.2–3.0] GeV/c for $K^+ + K^-$, and [0.3–4.6] GeV/c for $p + \overline{p}$.

3. Analysis and Results

The results obtained from combined minimum χ^2 fitting procedures using thermodynamically consistent and non-consistent Tsallis functions with transverse flow (functions in Equations (5) and (4), respectively) are presented in Tables 2 and 3, respectively. To show the quality of the combined fits with the functions in Equations (5) and (4), the experimental midrapidity transverse momentum distributions of the studied particle species in four centrality classes of Pb + Pb collisions at $\sqrt{s_{nn}}$ = 2.76 TeV, along with the resulting fit curves, are shown in Figures 1 and 2, respectively. As seen from Figures 1 and 2 and $\frac{\chi^2}{n.d.f.}$ values in Tables 2 and 3, the combined fits by both thermodynamically consistent and non-consistent Tsallis functions with transverse flow reproduce quite well the experimental midrapidity p_T distributions of the charged pions, kaons, and (anti)protons in 10 centrality groups of Pb + Pb collisions at $\sqrt{s_{nn}}$ = 2.76 TeV.

Table 2. The results obtained from combined minimum χ^2 fits with thermodynamically consistent Tsallis function with transverse flow (Equation (5)) of midrapidity p_T spectra of particles in Pb + Pb collisions at $\sqrt{s_{nn}}$ = 2.76 TeV. *n.d.f.* denotes the number of degrees of freedom.

Centrality	q $(\pi^+ + \pi^-)$	q $(K^+ + K^-)$	q $(p + \overline{p})$	T_0 (MeV)	$\langle\beta_T\rangle$	χ^2/*n.d.f.* (*n.d.f.*)
0–5%	1.084 ± 0.004	1.083 ± 0.004	1.082 ± 0.002	78 ± 3	0.60 ± 0.01	1.21 (100)
5–10%	1.087 ± 0.004	1.086 ± 0.004	1.085 ± 0.002	78 ± 3	0.58 ± 0.01	1.18 (100)
10–20%	1.091 ± 0.004	1.089 ± 0.004	1.086 ± 0.002	78 ± 3	0.58 ± 0.01	1.10 (100)
20–30%	1.097 ± 0.004	1.094 ± 0.004	1.089 ± 0.002	78 ± 3	0.55 ± 0.01	0.99 (100)
30–40%	1.103 ± 0.004	1.099 ± 0.003	1.092 ± 0.002	78 ± 3	0.52 ± 0.01	0.89 (100)
40–50%	1.111 ± 0.003	1.108 ± 0.003	1.098 ± 0.002	78 ± 3	0.47 ± 0.01	0.65 (100)
50–60%	1.118 ± 0.003	1.115 ± 0.003	1.103 ± 0.002	80 ± 3	0.40 ± 0.01	0.54 (100)
60–70%	1.126 ± 0.003	1.124 ± 0.002	1.108 ± 0.001	80 ± 3	0.33 ± 0.01	0.37 (100)
70–80%	1.133 ± 0.002	1.133 ± 0.002	1.112 ± 0.001	82 ± 3	0.24 ± 0.01	0.25 (100)
80–90%	1.139 ± 0.002	1.143 ± 0.002	1.114 ± 0.001	84 ± 3	0.12 ± 0.03	0.24 (101)

Table 3. The results obtained from combined minimum χ^2 fits with thermodynamically NON-consistent Tsallis function with transverse flow (Equation (4)) of midrapidity p_T spectra of particles in Pb + Pb collisions at $\sqrt{s_{nn}}$ = 2.76 TeV.

Centrality	q $(\pi^+ + \pi^-)$	q $(K^+ + K^-)$	q $(p + \overline{p})$	T_0 (MeV)	$\langle\beta_T\rangle$	χ^2/*n.d.f.* (*n.d.f.*)
0–5%	1.068 ± 0.006	1.068 ± 0.005	1.073 ± 0.003	120 ± 5	0.59 ± 0.01	1.02 (100)
5–10%	1.073 ± 0.006	1.072 ± 0.006	1.077 ± 0.003	121 ± 5	0.58 ± 0.01	1.01 (100)
10–20%	1.077 ± 0.006	1.076 ± 0.005	1.079 ± 0.003	121 ± 5	0.56 ± 0.01	0.93 (100)
20–30%	1.085 ± 0.006	1.082 ± 0.005	1.083 ± 0.003	122 ± 5	0.54 ± 0.01	0.99 (100)
30–40%	1.094 ± 0.006	1.091 ± 0.005	1.087 ± 0.003	123 ± 5	0.51 ± 0.01	0.74 (100)
40–50%	1.106 ± 0.005	1.102 ± 0.004	1.094 ± 0.002	124 ± 4	0.45 ± 0.01	0.53 (100)
50–60%	1.115 ± 0.005	1.113 ± 0.004	1.100 ± 0.002	129 ± 5	0.38 ± 0.01	0.43 (100)
60–70%	1.128 ± 0.004	1.127 ± 0.003	1.107 ± 0.002	130 ± 4	0.30 ± 0.01	0.29 (100)
70–80%	1.139 ± 0.003	1.141 ± 0.003	1.113 ± 0.002	134 ± 4	0.21 ± 0.01	0.20 (100)
80–90%	1.148 ± 0.003	1.156 ± 0.003	1.117 ± 0.002	137 ± 5	0.09 ± 0.02	0.21 (101)

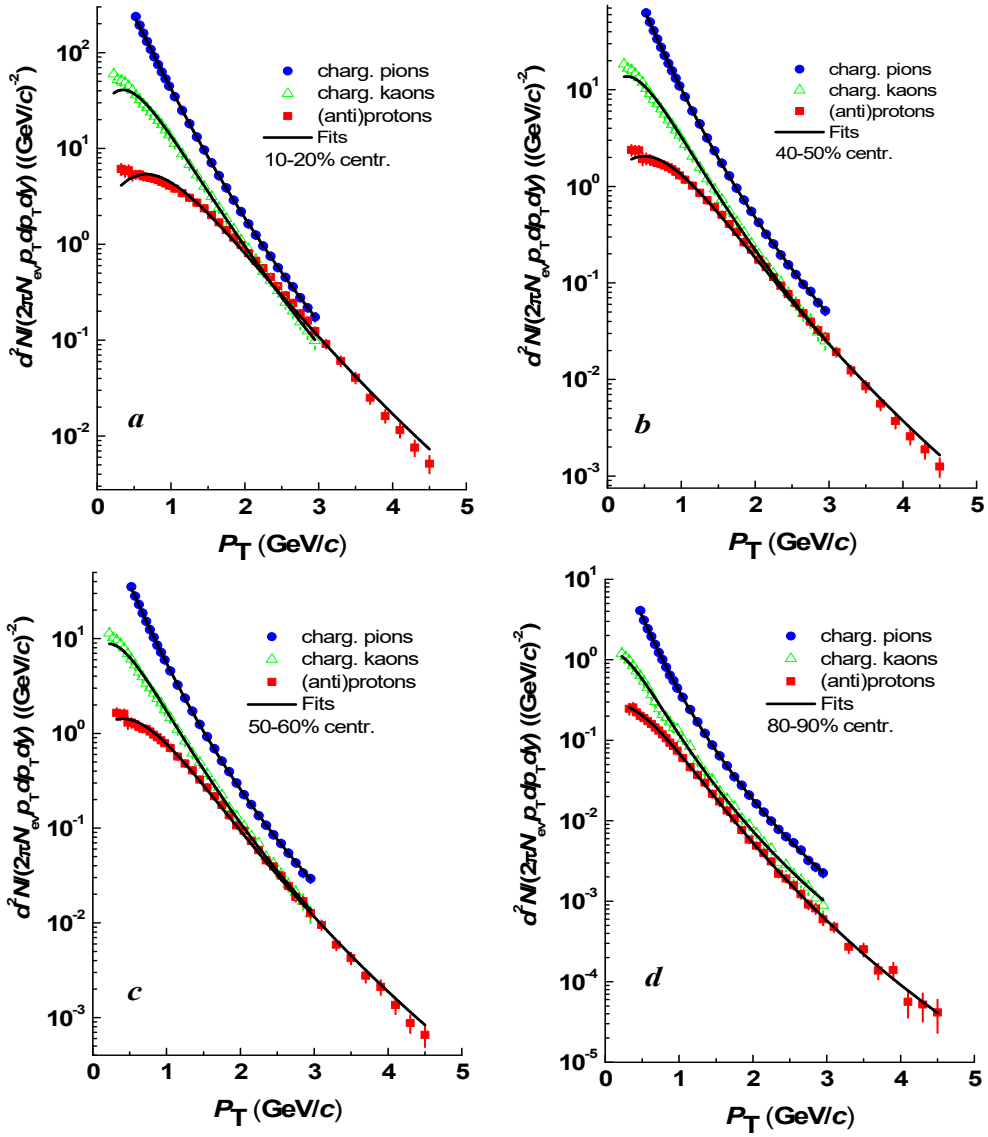

Figure 1. The resulting fit curves by Tsallis function with thermodynamical consistence with included transverse flow (Equation (5)) of the experimental midrapidity transverse momentum spectra of the charged pions (●), kaons (Δ), and protons and antiprotons (■) in Pb + Pb collisions at $\sqrt{s_{nn}}$ = 2.76 TeV at various centralities: 10–20% (**a**), 40–50% (**b**), 50–60% (**c**), and 80–90% (**d**).

The $\frac{\chi^2}{n.d.f.}$ values in Table 3 are slightly smaller than the corresponding values in Table 2, implying that, mathematically, the quality of the fits performed by non-consistent Tsallis function with transverse flow (Equation (4)) are slightly better than those performed by thermodynamically consistent Tsallis function with transverse flow (Equation (5)). However, from the physics perspective, it is preferable to use the thermodynamically consistent Tsallis function with transverse flow, because all the thermodynamic relations (those for the pressure, temperature, and particle and entropy densities) resulting from the first and second laws of thermodynamics are satisfied [38,43,44] by the thermodynamically consistent Tsallis function. Therefore, one can consider the temperature parameter T in the thermodynamically consistent Tsallis function [38] as being a true thermodynamic quantity.

To visualize and analyze the $\langle N_{part} \rangle$ dependencies of the parameters, the dependencies of q, T_0, and $\langle \beta_T \rangle$ on the average number of the participant nucleons, obtained from minimum χ^2 fits by thermodynamically consistent as well as non-consistent Tsallis function with transverse flow and given in Tables 2 and 3, are shown in Figure 3.

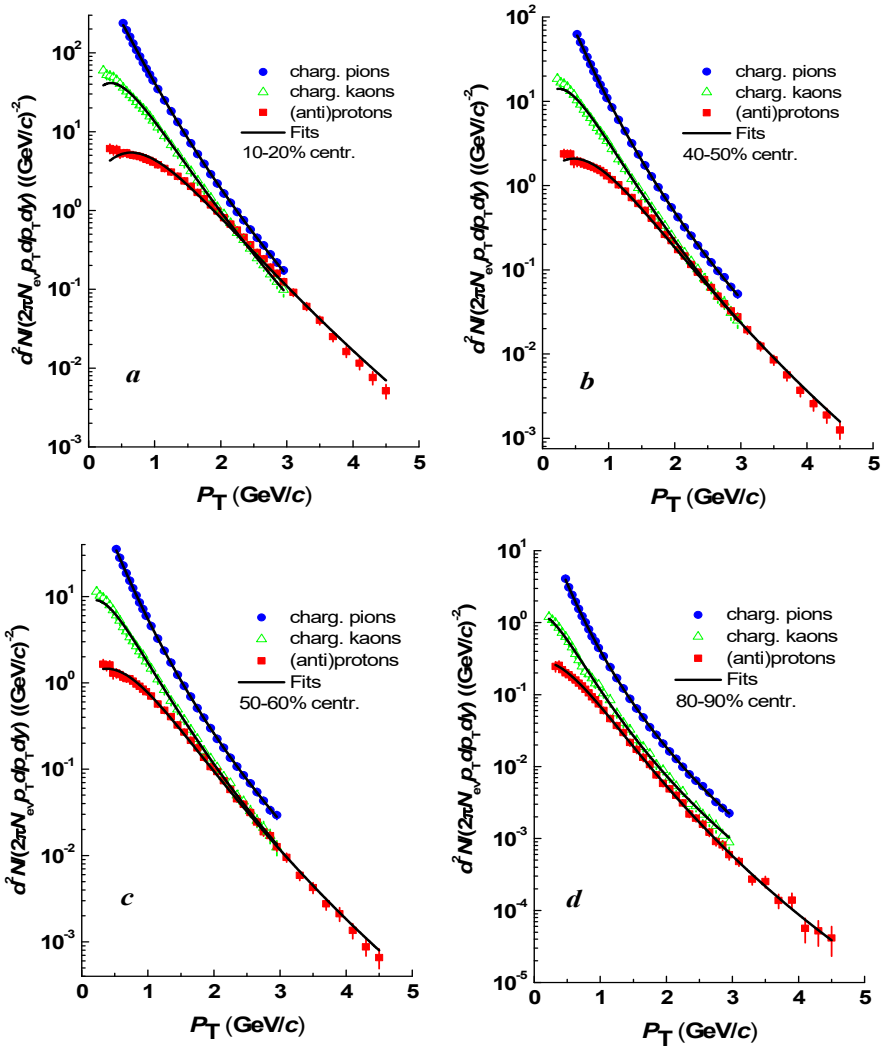

Figure 2. The resulting fit curves by non-consistent Tsallis function with included transverse flow (Equation (4)) of the experimental midrapidity transverse momentum spectra of the charged pions (●), kaons (Δ), and protons and antiprotons (■) in Pb + Pb collisions at $\sqrt{s_{nn}}$ = 2.76 TeV at various centralities: 10–20% (**a**), 40–50% (**b**), 50–60% (**c**), and 80–90% (**d**).

As seen from Figure 3a, the shapes of T_0 versus $\langle N_{part} \rangle$ dependencies are similar in case of fits by both thermodynamically consistent as well as non-consistent Tsallis function with transverse flow. At the same time, the absolute values of T_0 are consistently smaller in case of fits by the function in Equation (5), compared to those by the function in Equation (4), which is obviously due to the extra $\langle \gamma_T \rangle (m_T - p_T \langle \beta_T \rangle)$ factor in Equation (5) as compared to Equation (4). As observed from Figure 3a, the T_0 values decrease with increasing $\langle N_{part} \rangle$ in region $\langle N_{part} \rangle < 71$ and remain constant in region $\langle N_{part} \rangle > 71$. Additionally, as seen from Figure 3b, the parameter $\langle \beta_T \rangle$ shows significantly differing growth rates with increasing $\langle N_{part} \rangle$ in these two regions: a relatively higher increase rate in region $\langle N_{part} \rangle < 71$ and a smaller one in region $\langle N_{part} \rangle > 71$. The border $\langle N_{part} \rangle = 71 \pm 5$ between these two distinct regions was estimated as the middle value of $\langle N_{part} \rangle$ between the fourth and fifth points on Figure 3a, corresponding to the 50–60% and 40–50% centrality groups in Table 1. The corresponding border value $\langle dN_{ch}/d\eta \rangle = 205 \pm 15$ was calculated as the middle between the $\langle dN_{ch}/d\eta \rangle$ values for 50–60% and 40–50% centrality in Table 1. Analogously the corresponding border value of transverse flow velocity $\langle \beta_T \rangle = 0.44 \pm 0.02$ was estimated as the middle between the extracted $\langle \beta_T \rangle$ values for 50–60% and 40–50% centrality in Table 2. To quantify the different growth rates of $\langle \beta_T \rangle$ in regions $\langle N_{part} \rangle < 71$ and $\langle N_{part} \rangle > 71$, we

have fitted the $\langle \beta_T \rangle$ versus $\langle N_{part} \rangle$ dependence in Figure 3b, obtained from fitting with thermodynamically consistent Tsallis functions with transverse flow,

$$\begin{array}{c} \text{usingsingle-powerfunction} \\ \langle \beta_T \rangle = A \cdot \langle N_{part} \rangle^{\alpha} \cdot (A^{-} \text{ fitting constant, } \alpha^{-} \text{exponent parameter}) \\ \text{andtwo-powerfunction} \end{array} \quad (6)$$

$$\langle \beta_T \rangle = A_1 \cdot u\left(71 - \langle N_{part} \rangle\right) \cdot \langle N_{part} \rangle^{\alpha_1} + A_2 \cdot u\left(\langle N_{part} \rangle - 71\right) \cdot \langle N_{part} \rangle^{\alpha_2}, \quad (7)$$

where $u(t)$ is the Heaviside function ($u(t) = 0$ if $t < 0$, and $u(t) = 1$ if $t > 0$), A_1 and A_2—fitting (normalization) constants, and α_1 and α_2 are exponent parameters. The parameters of minimum χ^2 fits with the functions in Equations (6) and (7) of $\langle \beta_T \rangle$ versus $\langle N_{part} \rangle$ dependence in Figure 3b, obtained using a consistent Tsallis function with transverse flow, are given in Table 4. As seen in Table 4 and Figure 3b, the two-power function in Equation (7) fits the $\langle \beta_T \rangle$ versus $\langle N_{part} \rangle$ dependence quite well, while the single-power function in Equation (6) fails to fit this dependence.

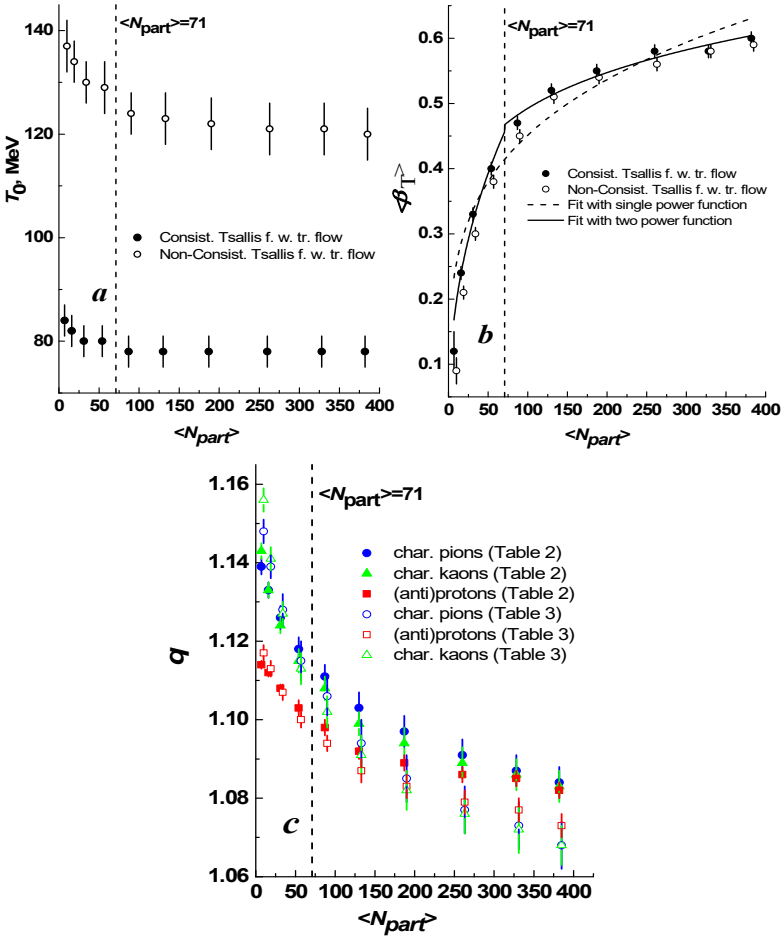

Figure 3. The $\langle N_{part} \rangle$ dependencies of the T_0 (**a**) and $\langle \beta_T \rangle$ (**b**) parameters (●) in Pb + Pb collisions at $\sqrt{s_{nn}}$ = 2.76 TeV extracted using Equation (5) and given in Table 2; (**c**)—the $\langle N_{part} \rangle$ dependence for the extracted q values given in Table 2 for the charged pions (●), kaons (▲), and protons and antiprotons (■). The results (Table 3) obtained for the respective particles in Pb + Pb collisions at $\sqrt{s_{nn}}$ = 2.76 TeV using Equation (4) are shown by the corresponding open symbols. The dashed and solid curves in panel (**b**) are minimum $\chi 2$ fits by the simple single-power (Equation (6)) and two-power (Equation (7)) functions, respectively, of the $\langle \beta_T \rangle$ versus $\langle N_{part} \rangle$ dependence, respectively, extracted using Equation (5). The data (open symbols), obtained using Equation (4), are slightly shifted along the positive direction of $\langle N_{part} \rangle$ axis for better visibility.

Table 4. The parameters of minimum χ^2 fits with the functions in Equations (6) and (7) of $\langle\beta_T\rangle$ versus $\langle N_{part}\rangle$ dependence in Figure 3b, obtained using consistent Tsallis function with transverse flow (Equation (5)).

Fitting Function	Parameter Values	χ^2/*n.d.f.* (*n.d.f.*)
Equation (6)	$A = 0.143 \pm 0.019$ $\alpha = 0.249 \pm 0.025$	10.68 (8)
Equation (7)	$A_1 = 0.073 \pm 0.012$ $\alpha_1 = 0.432 \pm 0.044$ $A_2 = 0.244 \pm 0.024$ $\alpha_2 = 0.152 \pm 0.018$	1.50 (6)

The obtained significantly different behavior of $\langle\beta_T\rangle$ versus $\langle N_{part}\rangle$ in regions $\langle N_{part}\rangle < 71$ and $\langle N_{part}\rangle > 71$ with the temperature parameter becoming constant in region $\langle N_{part}\rangle > 71$ could indicate that $\langle N_{part}\rangle = 71 \pm 5$ (corresponding to $\langle dN_{ch}/d\eta\rangle = 205 \pm 15$) is a border value of collision centrality for a crossover phase transition from the dense hadronic state to that of the QGP state (or mixed state of QGP and hadrons) in Pb + Pb collisions at $\sqrt{s_{nn}}$ = 2.76 TeV. It is important to note that the similar behaviors of $\langle\beta_T\rangle$ versus $\langle N_{part}\rangle$ as well as T_0 versus $\langle\beta_T\rangle$ dependencies with two distinct regions of $\langle N_{part}\rangle$ have been obtained recently in Refs. [18,33] from similar analyses, using the functions in Equations (4) and (5), of the experimental midrapidity transverse momentum distributions of identified charged particles in Xe + Xe collisions at $\sqrt{s_{nn}}$ = 5.44 TeV and Pb + Pb collisions at $\sqrt{s_{nn}}$ = 5.02 TeV. It is interesting to note that the corresponding border between two distinct $\langle N_{part}\rangle$ regions with significantly different behaviors of $\langle\beta_T\rangle$ versus $\langle N_{part}\rangle$ as well as T_0 versus $\langle N_{part}\rangle$ dependencies was found to be between the 50–60% and 40–50% centrality classes in both Xe + Xe collisions at $\sqrt{s_{nn}}$ = 5.44 TeV [18] and Pb + Pb collisions at $\sqrt{s_{nn}}$ = 5.02 TeV [33], coinciding with the corresponding border centrality intervals for Pb + Pb collisions at $\sqrt{s_{nn}}$ = 2.76 TeV in the present work. A comparison of the estimated border values of $\langle N_{part}\rangle$, $\langle dN_{ch}/d\eta\rangle$, and $\langle\beta_T\rangle$ for probable crossover phase transition from the dense hadronic state to that of the QGP state (or mixed state of QGP and hadrons) in the present work on Pb + Pb collisions at $\sqrt{s_{nn}}$ = 2.76 TeV with those estimated in Refs. [18,33] in Xe + Xe collisions at $\sqrt{s_{nn}}$ = 5.44 TeV and Pb + Pb collisions at $\sqrt{s_{nn}}$ = 5.02 TeV, respectively, is presented in Table 5.

Table 5. The comparison of the border values of $\langle N_{part}\rangle$, $\langle dN_{ch}/d\eta\rangle$, and $\langle\beta_t\rangle$, estimated in Pb + Pb collisions at $\sqrt{s_{nn}}$ = 2.76 TeV in the present work, with those extracted recently in Xe + Xe collisions at $(s_{\rm nn})^{1/2}$ = 5.44 TeV [18] and Pb + Pb collisions at $\sqrt{s_{nn}}$ = 5.02 TeV [33].

Quantity	Xe + Xe Collisions at $\sqrt{s_{nn}}$ = 5.44 TeV [18]	Pb + Pb Collisions at $\sqrt{s_{nn}}$ = 5.02 TeV [33]	Pb + Pb Collisions at $\sqrt{s_{nn}}$ = 2.76 TeV (Present Work)
$\langle N_{part}\rangle$	44 ± 5	71 ± 7	71 ± 5
$\langle dN_{ch}/d\eta\rangle$	158 ± 20	251 ± 20	205 ± 15
$\langle\beta_T\rangle$	0.44 ± 0.02	0.46 ± 0.03	0.44 ± 0.02

As seen from Table 5, the estimated border values of $\langle N_{part}\rangle$ in Pb + Pb collisions at $\sqrt{s_{nn}}$ = 2.76 and 5.02 TeV proved to be significantly larger compared to those in Xe + Xe collisions at $\sqrt{s_{nn}}$ = 5.44 TeV. This can be explained by the significant difference in the mass numbers, A, of the Pb and Xe nuclei, and hence the larger number of the participant nucleons in the overlap zone of colliding nuclei in case of Pb + Pb compared to Xe + Xe collisions for the border value between the 50–60% and 40–50% centrality classes, coinciding for these three collision types. The coincidence of the border values of $\langle N_{part}\rangle$ in Pb + Pb collisions at $\sqrt{s_{nn}}$ = 2.76 and 5.02 TeV is obviously due to the same collision system and geometry for the coinciding estimated border between the 50–60% and 40–50% centrality groups in both cases. It should be noted that the ratio (1.61 ± 0.24) of the evaluated

border values of $\langle N_{part} \rangle$ in Pb + Pb collisions at $\sqrt{s_{nn}}$ = 5.02 TeV and Xe + Xe collisions at $\sqrt{s_{nn}}$ = 5.44 TeV was found to coincide [33] with that (1.59 ± 0.24) of the respective border values of $\langle dN_{ch}/d\eta \rangle$ in these two collisions, and with the ratio of the mass numbers of the corresponding ^{208}Pb and ^{132}Xe nuclei equal to $\frac{A(208_{Pb})}{A(132_{Xe})} \approx 1.58$. The approximate relation $\frac{\langle N_{part} \rangle_{Pb+Pb}}{\langle N_{part} \rangle_{Xe+Xe}} \approx \frac{\langle dN_{ch}/d\eta \rangle_{Pb+Pb}}{\langle dN_{ch}/d\eta \rangle_{Xe+Xe}} \approx \frac{A(208_{Pb})}{A(132_{Xe})} \approx 1.6$ was satisfied [33] for the border values estimated in Pb + Pb and Xe + Xe collisions $\sqrt{s_{nn}}$ = 5.02 and 5.44 TeV, respectively, with the close values of the center-of-mass collision energy per nucleon pair. The significantly larger estimated border value $\langle dN_{ch}/d\eta \rangle = 251 \pm 20$ in Pb + Pb collisions at $\sqrt{s_{nn}}$ = 5.02 TeV as compared to $\langle dN_{ch}/d\eta \rangle = 205 \pm 15$ in Pb + Pb collisions at $\sqrt{s_{nn}}$ = 2.76 TeV, as seen in Table 5, is likely due to the significantly higher energy density (hence, larger charged-particle multiplicity density) and more particles produced in cases of significantly larger value of center-of-mass collision energy, $\sqrt{s_{nn}}$ = 5.02 TeV, per nucleon pair.

As seen from Figure 3c, the non-extensivity parameter q decreases systematically for all studied particle species with increasing the centrality of Pb + Pb collisions at $\sqrt{s_{nn}}$ = 2.76 TeV (with an increase in $\langle N_{part} \rangle$). Figure 3c also shows that the rate of decrease of q with increasing $\langle N_{part} \rangle$ in region $\langle N_{part} \rangle < 71$ is noticeably greater than that in range $\langle N_{part} \rangle > 71$. It is seen that q for pions coincides within uncertainties with q for kaons in the whole range of $\langle N_{part} \rangle$, and in region $\langle N_{part} \rangle < 100$ the parameter q for (anti)protons is noticeably smaller than q for pions and kaons. It agrees well with the relation q(baryons) < q(mesons) obtained earlier in high-energy collisions in Refs. [17–19,28,33,45,46,48,49]. However, as observed from Figure 3c, on the whole the gap between parameter q for mesons and baryons decreases with increasing $\langle N_{part} \rangle$, and q for all studied particle species, i.e., for pions, kaons, and (anti)protons, becomes the same within uncertainties in region $\langle N_{part} \rangle > 160$, in good agreement with the similar result obtained in Pb + Pb collisions at $\sqrt{s_{nn}}$ = 5.02 TeV in recent work [33]. The observed coincidence of the q parameter for the charged pions and kaons, protons and antiprotons at large $\langle N_{part} \rangle$ indicates likely that the highly thermalized and equilibrated QGP is produced in central Pb + Pb collisions at $\sqrt{s_{nn}}$ = 2.76 TeV with $\langle N_{part} \rangle > 160$ in agreement with the similar result found in central Pb + Pb collisions at $\sqrt{s_{nn}}$ = 5.02 TeV in Ref. [33]. The similar decrease, with increasing $\langle N_{part} \rangle$, of the gap between q for (anti)protons, on the one hand, and q for pions and kaons, on the other hand, with parameter q coinciding for these mesons and baryons at large $\langle N_{part} \rangle$ was also observed in Xe + Xe collisions at $\sqrt{s_{nn}}$ = 5.44 TeV in Ref. [18].

Currently, it is important to study the correlations between the extracted parameters. The T_0 versus $\langle \beta_T \rangle$ dependencies, obtained from fits by non-consistent as well as thermodynamically consistent Tsallis function with transverse flow and presented in Tables 2 and 3, are shown in Figure 4a,b, respectively. The obtained Pearson linear correlation coefficient, r_{xy}, between two parameters and the one-sigma confidence ellipse (covering a 68% confidence interval) of the covariance of the T_0 and $\langle \beta_T \rangle$ parameters are also shown in Figure 4. The corresponding 1-sigma confidence ellipse and calculated r_{xy} coefficient of a linear correlation between pairs of parameters are also presented in Figure 4. The Pearson correlation coefficient, r_{xy}, shows the magnitude of a linear correlation between two parameter sets, and it can vary between −1 and +1 values. The r_{xy} equal to −1 and +1 corresponds to the full negative linear correlation (anticorrelation) and full positive linear correlation, respectively, whereas $r_{xy} = 0$ denotes the absence of a linear correlation between two sets of data. As seen from the orientations and shapes of confidence ellipses and corresponding r_{xy} values in Figure 4a,b, the parameters T_0 and $\langle \beta_T \rangle$ are highly anticorrelated. As observed from Figure 4a,b, the T_0 versus $\langle \beta_T \rangle$ dependencies differ in regions $\langle \beta_T \rangle < 0.44$ and $\langle \beta_T \rangle > 0.44$, corresponding to Pb + Pb collisions at $\sqrt{s_{nn}}$ = 2.76 TeV with $\langle N_{part} \rangle < 71$ and $\langle N_{part} \rangle > 71$, respectively. The T_0 versus $\langle \beta_T \rangle$ dependence (from Figure 4a) is shown separately for regions $\langle \beta_T \rangle < 0.44$ and $\langle \beta_T \rangle > 0.44$ in Figure 5a,b, respectively. As seen from Figure 5a, the T_0 and $\langle \beta_T \rangle$ parameters are strongly anticorrelated in region $\langle \beta_T \rangle < 0.44$. On the other hand, as observed from Figure 5b, the linear correlation between T_0 and $\langle \beta_T \rangle$ is practically absent in region $\langle \beta_T \rangle > 0.44$. The similar result has been obtained recently in

Pb + Pb collisions at $\sqrt{s_{nn}}$ = 5.02 TeV [33] and Xe + Xe collisions at $\sqrt{s_{nn}}$ = 5.44 TeV [18]. Thus, in addition to significantly different growth rates of $\langle \beta_T \rangle$ in regions $\langle N_{part} \rangle < 71 \pm 5$ and $\langle N_{part} \rangle > 71 \pm 5$, we have observed the considerably different correlations between T_0 and $\langle \beta_T \rangle$ parameters in corresponding $\langle \beta_T \rangle < 0.44$ and $\langle \beta_T \rangle > 0.44$ ranges. This further substantiates our assumption that $\langle N_{part} \rangle \approx 71 \pm 5$ ($\langle dN_{ch}/d\eta \rangle \approx 205 \pm 15$) could be a border value of collision centrality for crossover transition from dense hadronic phase to the QGP state (or mixed state of QGP and hadrons) in Pb + Pb collisions at $\sqrt{s_{nn}}$ = 2.76 TeV.

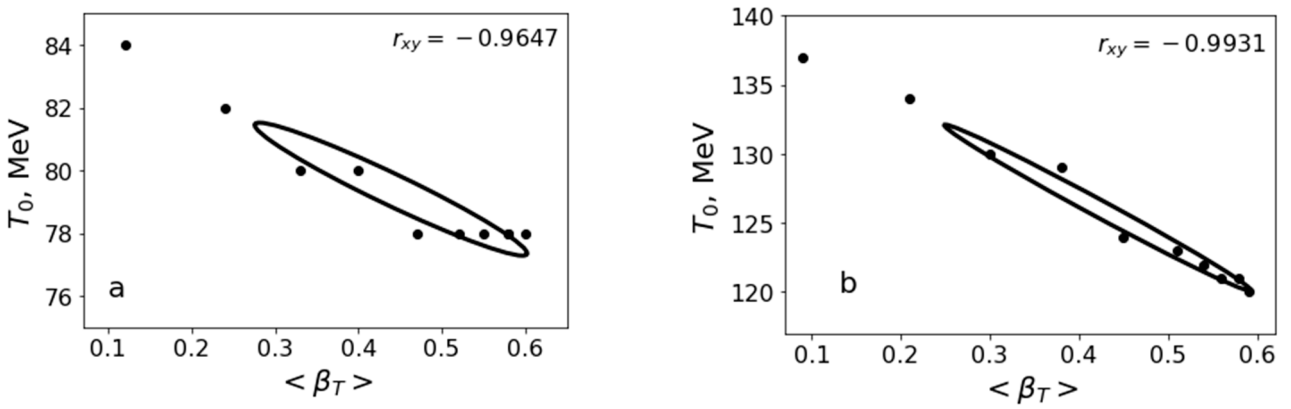

Figure 4. (**a**)—Dependence (•) of T_0 versus $\langle \beta_T \rangle$ parameters extracted using Equation (5) and presented in Table 2. (**b**)—Dependence (•) of T_0 versus $\langle \beta_T \rangle$ parameters extracted using Equation (4) and presented in Table 3. The 1-sigma confidence ellipse (which corresponds to a 68% confidence interval) of the covariance of parameters T_0 and $\langle \beta_T \rangle$ and the calculated Pearson correlation coefficient, r_{xy}, between T_0 and $\langle \beta_T \rangle$ are also given in the figures.

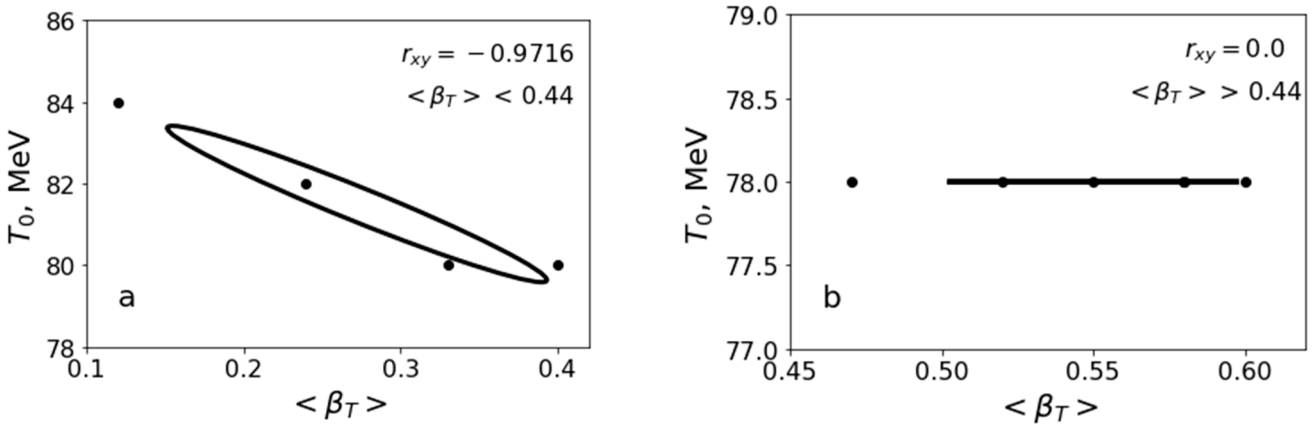

Figure 5. (**a**)—Dependence (•) of T_0 versus $\langle \beta_T \rangle$ parameters, extracted using Equation (5) and presented in Table 2, in region $\langle \beta_T \rangle < 0.44$. (**b**)—Dependence (•) of T_0 versus $\langle \beta_T \rangle$ parameters, extracted using Equation (5) and presented in Table 2, in region $\langle \beta_T \rangle > 0.44$. The corresponding 1-sigma confidence ellipses and Pearson correlation coefficients are also shown in the figures.

It is important to also check the correlations between other pairs of the parameters in Table 2, extracted using a thermodynamically consistent Tsallis function with transverse flow. The q(pions) versus q(kaons), q(pions) versus q((anti)protons), and q(kaons) versus q((anti)protons) dependencies are shown in Figure 6a–c, respectively. The q(pions) versus $\langle \beta_T \rangle$, q((anti)protons) versus $\langle \beta_T \rangle$, and q(kaons) versus $\langle \beta_T \rangle$ dependencies are illustrated in Figure 7a–c, respectively. The q(pions) versus T_0, q((anti)protons) versus T_0, and q(kaons) versus T_0 dependencies are displayed in Figure 8a–c, respectively.

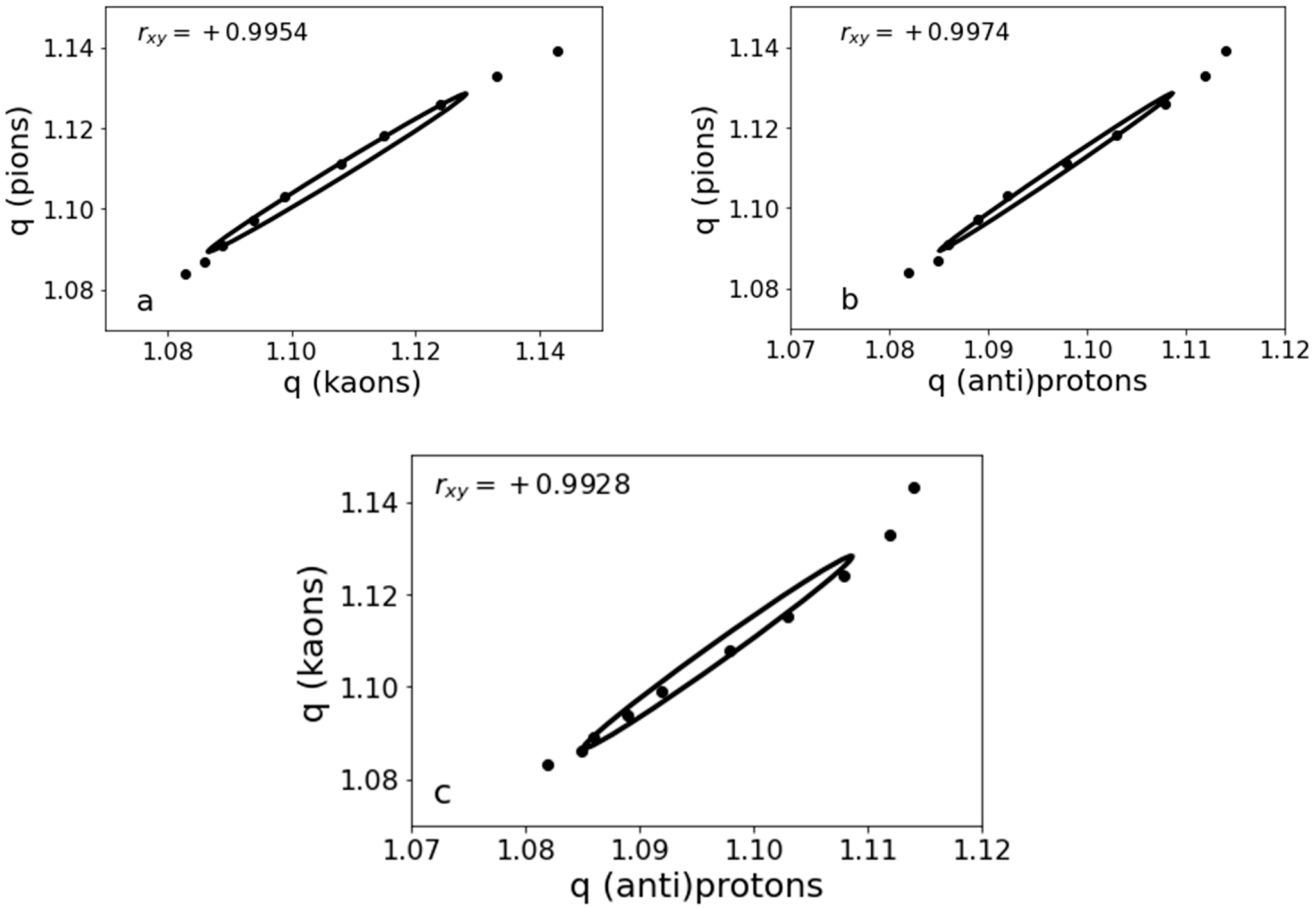

Figure 6. The q(pions) versus q(kaons) (**a**), q(pions) versus q((anti)protons) (**b**), and q(kaons) versus q((anti)protons) (**c**) dependencies, obtained using Equation (5) and presented in Table 2. The corresponding 1-sigma confidence ellipses and Pearson correlation coefficients are also shown in the figures.

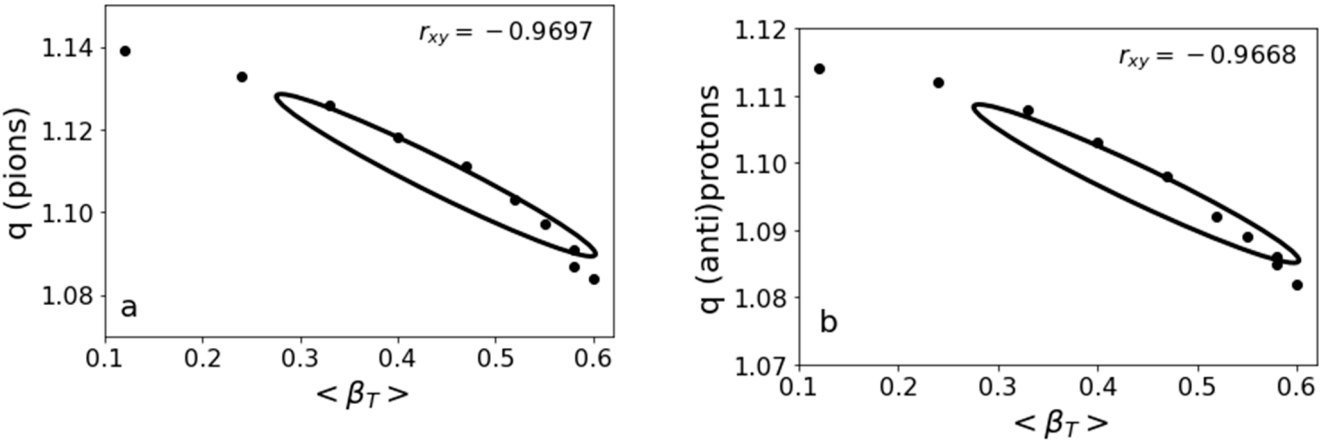

Figure 7. *Cont.*

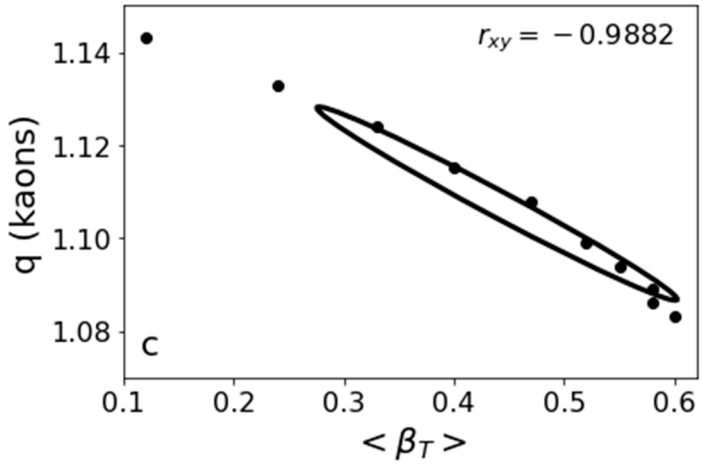

Figure 7. The q(pions) versus $\langle \beta_T \rangle$ (**a**), q((anti)protons) versus $\langle \beta_T \rangle$ (**b**), and q(kaons) versus $\langle \beta_T \rangle$ (**c**) dependencies, obtained using Equation (5) and presented in Table 2. The corresponding 1-sigma confidence ellipses and Pearson correlation coefficients are also shown in the figures.

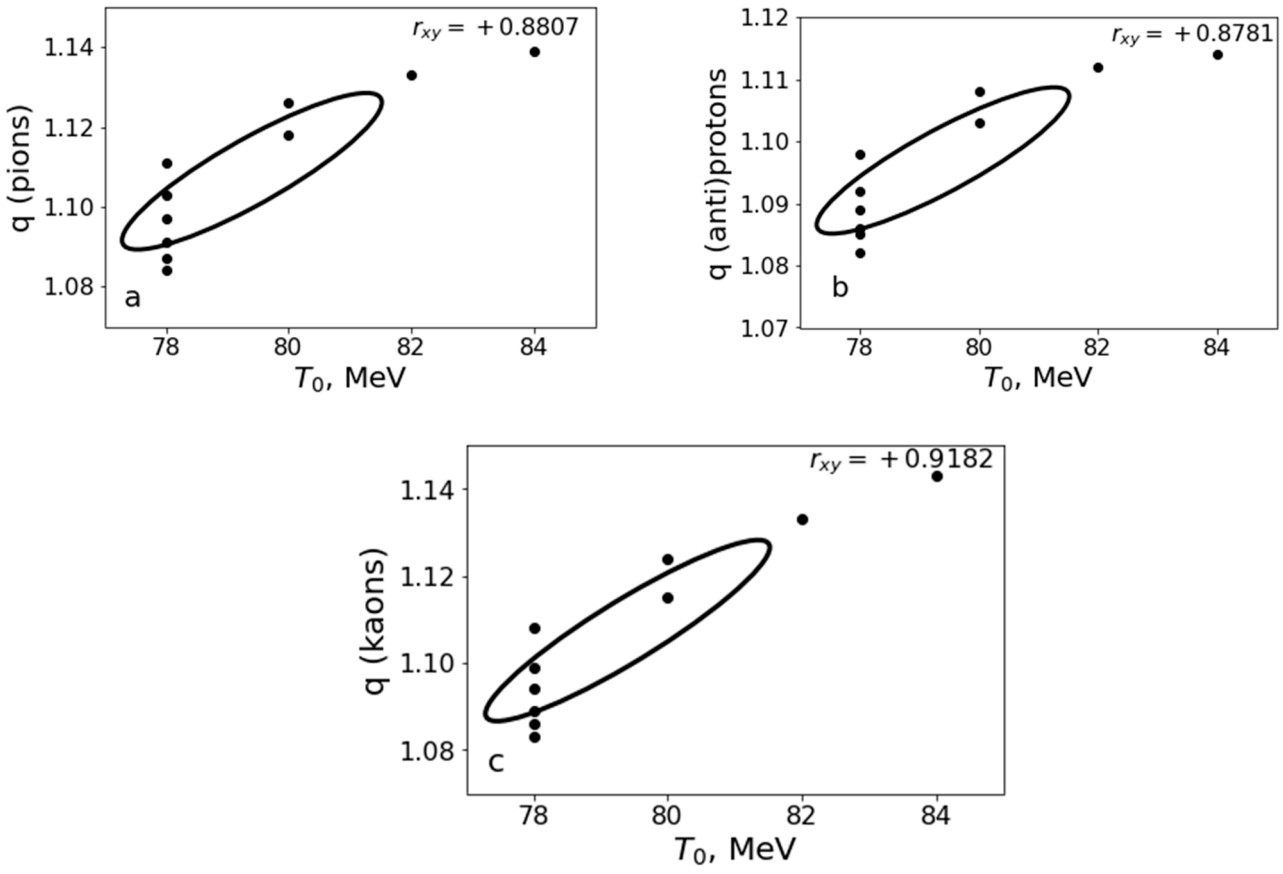

Figure 8. The q(pions) versus T_0 (**a**), q((anti)protons) versus T_0 (**b**), and q(kaons) versus T_0 (**c**) dependencies, obtained using Equation (5) and presented in Table 2. The corresponding 1-sigma confidence ellipses and Pearson correlation coefficients are also shown in the figures.

As seen from Figure 6a–c, the non-extensivity parameter q for pions and kaons, for pions and (anti) protons, as well as q for kaons and (anti) protons show the strong positive linear correlation with the Pearson correlation coefficient being very close to +1 for each pair of particle species. Figure 7a–c show that the non-extensivity parameter q is strongly negatively correlated (anticorrelated) with the average transverse flow velocity, $\langle \beta_T \rangle$, for all

studied particle species, with the Pearson correlation coefficient being close to -1 in each case. On the other hand, as seen from Figure 8a–c, quite a large positive linear correlation ($r_{xy} \approx +0.9$) exists between the q and temperature parameter T_0 in all three cases.

4. Summary and Conclusions

We have successfully analyzed the midrapidity transverse momentum distributions of the charged pions, kaons, protons, and antiprotons in 10 groups of centrality of Pb + Pb collisions at $\sqrt{s_{nn}}$ = 2.76 TeV, measured by the ALICE Collaboration, using both thermodynamically consistent and non-consistent Tsallis distribution function with embedded transverse flow. We have performed the combined minimum χ^2 fits by the above model functions of the experimental midrapidity p_T spectra of the analyzed particle species in each centrality class of Pb + Pb collisions to extract the global parameters T_0 and $\langle\beta_T\rangle$ of the system as well as non-extensivity parameter q for each particle type and study their dependencies on collision centrality ($\langle N_{part}\rangle$).

We have observed significantly different behavior (growth rates) of $\langle\beta_T\rangle$ in regions $\langle N_{part}\rangle < 71$ and $\langle N_{part}\rangle > 71$ with the temperature parameter becoming constant in region $\langle N_{part}\rangle > 71$. This could indicate that $\langle N_{part}\rangle = 71 \pm 5$ (corresponds to $\langle dN_{ch}/d\eta\rangle = 205 \pm 15$) is an estimated border value of collision centrality for crossover phase transition from the dense hadronic state to that of QGP state (or mixed state of QGP and hadrons) in Pb + Pb collisions at $\sqrt{s_{nn}}$ = 2.76 TeV.

The respective border between the two distinct $\langle N_{part}\rangle$ regions with different behaviors of $\langle\beta_T\rangle$ versus $\langle N_{part}\rangle$ as well as T_0 versus $\langle N_{part}\rangle$ dependencies was found to be between the 50–60% and 40–50% centrality classes in Pb + Pb collisions at $\sqrt{s_{nn}}$ = 2.76 TeV, coinciding with the corresponding border found to be also between 50–60% and 40–50% centrality in recent works [18,33] in both Xe + Xe collisions at $\sqrt{s_{nn}}$ = 5.44 TeV and Pb + Pb collisions at $\sqrt{s_{nn}}$ = 5.02 TeV. The coincidence of the border values of $\langle N_{part}\rangle$ in Pb + Pb collisions at $\sqrt{s_{nn}}$ = 2.76 and 5.02 TeV has been observed, which is due to the same collision system and geometry. The estimated border values of $\langle N_{part}\rangle$ in Pb + Pb collisions at $\sqrt{s_{nn}}$ = 2.76 and 5.02 TeV have been significantly larger compared to that in Xe + Xe collisions at $\sqrt{s_{nn}}$ = 5.44 TeV. The significantly larger estimated border value $\langle dN_{ch}/d\eta\rangle = 251 \pm 20$ in Pb + Pb collisions at $\sqrt{s_{nn}}$ = 5.02 TeV as compared to $\langle dN_{ch}/d\eta\rangle = 205 \pm 15$ in Pb + Pb collisions at $\sqrt{s_{nn}}$ = 2.76 TeV could be explained by the significantly greater energy density (hence, larger charged-particle multiplicity density) and more particles produced in case of significantly larger value of center-of-mass collision energy, $\sqrt{s_{nn}}$ = 5.02 TeV, per nucleon pair.

The non-extensivity parameter q has decreased systematically for all studied particle species with the increasing centrality of Pb + Pb collisions at $\sqrt{s_{nn}}$ = 2.76 TeV in agreement with the similar tendency observed in recent works in Xe + Xe collisions at $\sqrt{s_{nn}}$ = 5.44 TeV as well as Pb + Pb collisions at $\sqrt{s_{nn}}$ = 5.02 TeV. The gap between q(mesons) and q(baryons) has decreased with an increase in $\langle N_{part}\rangle$. We have observed coincidence of the q parameter for the analyzed mesons and baryons in more central collisions with large $\langle N_{part}\rangle$, suggesting that the highly thermalized and equilibrated QGP is produced in central Pb + Pb collisions at $\sqrt{s_{nn}}$ = 2.76 TeV with $\langle N_{part}\rangle > 160$.

The T_0 and $\langle\beta_T\rangle$ parameters are strongly anticorrelated in region $\langle\beta_T\rangle < 0.44$, and the linear correlation between T_0 and $\langle\beta_T\rangle$ is practically absent in region $\langle\beta_T\rangle > 0.44$. Hence, besides significantly different growth rates of $\langle\beta_T\rangle$ in regions $\langle N_{part}\rangle < 71 \pm 5$ and $\langle N_{part}\rangle > 71 \pm 5$, we have obtained considerably different correlations between T_0 and $\langle\beta_T\rangle$ parameters in the corresponding $\langle\beta_T\rangle < 0.44$ and $\langle\beta_T\rangle > 0.44$ ranges. This further supports our finding that $\langle N_{part}\rangle \approx 71 \pm 5$ ($\langle dN_{ch}/d\eta\rangle \approx 205 \pm 15$) could be a border value of collision centrality for crossover transition from dense hadronic phase to the QGP state (or mixed state of QGP and hadrons) in Pb + Pb collisions at $\sqrt{s_{nn}}$ = 2.76 TeV.

The strong positive linear correlation between non-extensivity parameter q for pions and kaons, between q for pions and (anti) protons, and between q for kaons and (anti)protons has been obtained with the corresponding Pearson correlation coefficient, r_{xy},

being very close to +1 for each pair of particle species. On the other hand, the parameter q for all studied particle species has proved to be strongly negatively correlated (anticorrelated) with the average transverse flow velocity, $\langle\beta_T\rangle$, with r_{xy} being close to -1 in each case. Quite a large positive linear correlation ($r_{xy} \approx +0.9$) has been observed between the q for the studied particle species and temperature parameter, T_0.

Author Contributions: All authors have contributed equally to this work. All authors have read and agreed to the published version of the manuscript.

Funding: This research was funded by the Science Committee of the Ministry of Education and Science of the Republic of Kazakhstan (Grant No. AP14869032). The work of PTI authors was supported by the Ministry of Innovative Development of Uzbekistan within the fundamental project № F3-20200929146 on analysis of open data on heavy-ion collisions at the LHC. The work of F.-H.L. was supported by the National Natural Science Foundation of China under Grant № 11575103 and the Shanxi Provincial Natural Science Foundation under Grant № 201901D111043.

Data Availability Statement: The data analyzed in this article are included within the paper and cited as references at relevant places within the text of the manuscript.

Conflicts of Interest: The authors do not have any conflict of interest regarding the article.

References

1. Heinz, U.W.; Jacob, M. Evidence for a New State of Matter: An Assessment of the Results from the CERN Lead Beam Programme. *arXiv* **2000**, arXiv:nucl-th/0002042.
2. BRAHMS Collab. Quark–gluon plasma and color glass condensate at RHIC? The perspective from the BRAHMS experiment. *Nucl. Phys. A* **2005**, *757*, 1–27. [CrossRef]
3. PHENIX Collab. Formation of dense partonic matter in relativistic nucleus–nucleus collisions at RHIC: Experimental evaluation by the PHENIX Collaboration. *Nucl. Phys. A* **2005**, *757*, 184. [CrossRef]
4. Back, B.B.; Baker, M.D.; Ballintijn, M.; Barton, D.S.; Becker, B.; Betts, R.R.; Bickley, A.A.; Bindel, R.; Budzanowski, A.; Busza, W.; et al. The PHOBOS perspective on discoveries at RHIC. *Nucl. Phys. A* **2005**, *757*, 28–101. [CrossRef]
5. STAR Collab. Experimental and theoretical challenges in the search for the quark–gluon plasma: The STAR Collaboration's critical assessment of the evidence from RHIC collisions. *Nucl. Phys. A* **2005**, *757*, 102–183. [CrossRef]
6. Shuryak, E.V. What RHIC experiments and theory tell us about properties of quark–gluon plasma? *Nucl. Phys. A* **2005**, *750*, 64–83. [CrossRef]
7. CMS Collab. Observation and studies of jet quenching in PbPb collisions at $\sqrt{s_{nn}}$ = 2.76 TeV. *Phys. Rev. C* **2011**, *84*, 024906.
8. Song, H.; Bass, S.A.; Heinz, U.; Hirano, T.; Shen, C. 200 A GeV Au+Au Collisions Serve a Nearly Perfect Quark-Gluon Liquid. *Phys. Rev. Lett.* **2011**, *106*, 192301. [CrossRef]
9. Rafelski, J. Melting hadrons, boiling quarks. *Eur. Phys. J. A* **2015**, *51*, 114. [CrossRef]
10. STAR Collab. Bulk Properties of the Medium Produced in Relativistic Heavy-Ion Collisions from the Beam Energy Scan Program. *Phys. Rev. C* **2017**, *96*, 044904. [CrossRef]
11. Braun-Munzinger, P.; Redlich, K.; Stachel, J. Particle production in heavy ion collisions. In *Quark Gluon Plasma 3*; Hwa, R.C., Wang, X.N., Eds.; World Scientific Publishing: Singapore, 2004.
12. Andronic, A.; Braun-Munzinger, P.; Stachel, J. Hadron production in central nucleus-nucleus collisions at chemical freezeout. *Nucl. Phys. A* **2006**, *772*, 167–199. [CrossRef]
13. Becattini, F.; Manninen, J.; Gazdzicki, M. Energy and system size dependence of chemical freeze-out in relativistic nuclear collisions. *Phys. Rev. C* **2006**, *73*, 044905. [CrossRef]
14. Andronic, A.; Braun-Munzinger, P.; Stachel, J. Thermal hadron production in relativistic nuclear collisions: The Hadron mass spectrum, the horn, and the QCD phase transition. *Phys. Lett. B* **2009**, *673*, 142–145. [CrossRef]
15. Stachel, J.; Andronic, A.; Braun-Munzinger, P.; Redlich, K. Confronting LHC data with the statistical hadronization model. In *Journal of Physics: Conference Series*; IOP Publishing: Bristol, UK, 2014; Volume 509, p. 012019.
16. ALICE Collab. Centrality dependence of π, K, p production in Pb-Pb collisions at $\sqrt{s_{nn}}$ = 2.76 TeV. *Phys. Rev. C* **2013**, *88*, 044910.
17. Olimov, K.K.; Liu, F.H.; Musaev, K.A.; Shodmonov, M.Z. Multiplicity Dependencies of Midrapidity Transverse Momentum Distributions of Identified Charged Particles in proton-proton Collisions at $(s)^{1/2}$=7 TeV at the LHC. *Universe* **2022**, *8*, 174. [CrossRef]
18. Olimov, K.K.; Liu, F.H.; Musaev, K.A.; Olimov, K.; Shodmonov, M.Z.; Fedosimova, A.I.; Lebedev, I.A.; Kanokova, S.Z.; Tukhtaev, B.J.; Yuldashev, B.S. Study of midrapidity p_t distributions of identified charged particles in Xe+Xe collisions at $(s_{nn})^{1/2}$=5.44 TeV using non-extensive Tsallis statistics with transverse flow. *Mod. Phys. Lett. A* **2022**, *37*, 2250095. [CrossRef]
19. Olimov, K.K.; Liu, F.H.; Musaev, K.A.; Olimov, K.; Tukhtaev, B.J.; Yuldashev, B.S.; Saidkhanov, N.S.; Umarov, K.I.; Gulamov, K.G. Multiplicity dependencies of midrapidity transverse momentum spectra of identified charged particles in p+p collisions at $(s)^{1/2}$=13 TeV at LHC. *Int. J. Mod. Phys. A* **2021**, *36*, 2150149. [CrossRef]

20. Zhang, Q.; Gao, Y.Q.; Liu, F.H.; Olimov, K.K. An Energy Independent Scaling of Transverse Momentum Spectra of Direct (Prompt) Photons from Two-Body Processes in High-Energy Proton–Proton Collisions. *Ann. Phys.* **2022**, *534*, 2100567. [CrossRef]
21. Schnedermann, E.; Sollfrank, J.; Heinz, U. Thermal phenomenology of hadrons from 200 A GeV S+S collisions. *Phys. Rev. C* **1993**, *48*, 2462. [CrossRef]
22. ALICE Collab. Production of charged pions, kaons and (anti-)protons in Pb-Pb and inelastic pp collisions at $\sqrt{s_{nn}}$ = 5.02 TeV. *Phys. Rev. C* **2020**, *101*, 044907.
23. STAR Collab. Systematic measurements of identified particle spectra in pp, d+Au, and Au+Au collisions at the STAR detector. *Phys. Rev. C* **2009**, *79*, 034909. [CrossRef]
24. STAR Collab. Identified particle production, azimuthal anisotropy, and interferometry measurements in Au+Au collisions at $\sqrt{s_{nn}}$ = 9.2 GeV. *Phys. Rev. C* **2010**, *81*, 024911.
25. Tang, Z.; Xu, Y.; Ruan, L.; van Buren, G.; Wang, F.; Xu, Z. Spectra and radial flow in relativistic heavy ion collisions with Tsallis statistics in a blast-wave description. *Phys. Rev. C* **2009**, *79*, 051901.
26. Lao, H.L.; Liu, F.H.; Lacey, R.A. Extracting kinetic freeze-out temperature and radial flow velocity from an improved Tsallis distribution. *Eur. Phys. J. A* **2017**, *53*, 44. [CrossRef]
27. Khandai, P.K.; Sett, P.; Shukla, P.; Singh, V. System size dependence of hadron pT spectra in p+p and Au+Au collisions at $\sqrt{s_{nn}}$ = 200 GeV. *J. Phys. G* **2014**, *41*, 025105.
28. Olimov, K.K.; Kanokova, S.Z.; Olimov, A.K.; Umarov, K.I.; Tukhtaev, B.J.; Gulamov, K.G.; Yuldashev, B.S.; Lutpullaev, S.L.; Saidkhanov, N.S.; Olimov, K.; et al. Combined analysis of midrapidity transverse momentum spectra of the charged pions and kaons, protons and antiprotons in p+p and Pb + Pb collisions at $(s_{nn})^{1/2}$= 2.76 and 5.02 TeV at the LHC. *Mod. Phys. Lett. A* **2020**, *35*, 2050237. [CrossRef]
29. Olimov, K.K.; Kanokova, S.Z.; Olimov, K.; Gulamov, K.G.; Yuldashev, B.S.; Lutpullaev, S.L.; Umarov, F.Y. Average transverse expansion velocities and global freeze-out temperatures in central Cu+Cu, Au+Au, and Pb + Pb collisions at high energies at RHIC and LHC. *Mod. Phys. Lett. A* **2020**, *35*, 2050115. [CrossRef]
30. Zhang, X.; Liu, F.; Olimov, K.K. A systematic analysis of transverse momentum spectra of J/ψ mesons in high energy collisions. *Int. J. Mod. Phys. E* **2021**, *30*, 2150051. [CrossRef]
31. Li, L.; Liu, F.; Olimov, K.K. Excitation Functions of Tsallis-Like Parameters in High-Energy Nucleus–Nucleus Collisions. *Entropy* **2021**, *23*, 478. [CrossRef]
32. Qi-Wang; Liu, F.; Olimov, K.K. Initial-State Temperature of Light Meson Emission Source from Squared Momentum Transfer Spectra in High-Energy Collisions. *Front. Phys.* **2021**, *9*, 792039. [CrossRef]
33. Olimov, K.K.; Liu, F.-H.; Fedosimova, A.I.; Lebedev, I.A.; Deppman, A.; Musaev, K.A.; Shodmonov, M.Z.; Tukhtaev, B.J. Analysis of Midrapidity p_T Distributions of Identified Charged Particles in Pb + Pb Collisions at $(s_{nn})^{1/2}$ = 5.02 TeV Using Tsallis Distribution with Embedded Transverse Flow. *Universe* **2022**, *8*, 401. [CrossRef]
34. Tsallis, C. Enthusiasm and Skepticism: Two Pillars of Science—A Nonextensive Statistics Case. *Physics* **2022**, *4*, 609–632. [CrossRef]
35. Rocha, L.Q. Nonextensive Statistics in High Energy Collisions. *Physics* **2022**, *4*, 659–671. [CrossRef]
36. Tsallis, C. Possible generalization of Boltzmann-Gibbs statistics. *J. Statist. Phys.* **1988**, *52*, 479–487. [CrossRef]
37. Tsallis, C. Nonadditive entropy: The concept and its use. *Eur. Phys. J. A* **2009**, *40*, 257–266. [CrossRef]
38. Cleymans, J.; Worku, D. The Tsallis distribution in proton–proton collisions at $(s)^{1/2}$= 0.9 TeV at the LHC. *J. Phys. G* **2012**, *39*, 025006. [CrossRef]
39. Sena, I.; Deppman, A. Systematic analysis of p_T -distributions in p+p collisions. *Eur. Phys. J. A* **2013**, *49*, 17. [CrossRef]
40. PHENIX Collab. Measurement of neutral mesons in p+p collisions at $(s)^{1/2}$=200 GeV and scaling properties of hadron production. *Phys. Rev. D* **2011**, *83*, 052004. [CrossRef]
41. Khandai, P.K.; Sett, P.; Shukla, P.; Singh, V. Hadron spectra in p+p collisions at RHIC and LHC energies. *Int. J. Mod. Phys. A* **2013**, *28*, 1350066. [CrossRef]
42. Wong, C.Y.; Wilk, G. Tsallis Fits to p_T Spectra for *pp* Collisions at LHC. *Acta Phys. Polon. B* **2012**, *43*, 2047. [CrossRef]
43. Cleymans, J.; Lykasov, G.I.; Parvan, A.S.; Sorin, A.S.; Teryaev, O.V.; Worku, D. Systematic properties of the Tsallis Distribution: Energy Dependence of Parameters in High-Energy p-p Collisions. *Phys. Lett. B* **2013**, *723*, 351–354. [CrossRef]
44. Cleymans, J. On the Use of the Tsallis Distribution at LHC Energies. *J. Phys. Conf. Ser.* **2017**, *779*, 012079. [CrossRef]
45. Zheng, H.; Zhu, L. Comparing the Tsallis Distribution with and without Thermodynamical Description in p-p Collisions. *Adv. High Energy Phys.* **2016**, *2016*, 9632126. [CrossRef]
46. Bíró, G.; Barnaföldi, G.G.; Biró, T.S.; Ürmössy, K.; Takács, Á. Systematic Analysis of the Non-Extensive Statistical Approach in High Energy Particle Collisions-Experiment vs. Theory. *Entropy* **2017**, *19*, 88. [CrossRef]
47. Wilk, G.; Wlodarczyk, Z. Interpretation of the Nonextensivity Parameter q in Some Applications of Tsallis Statistics and Lévy Distributions. *Phys. Rev. Lett.* **2000**, *84*, 2770. [CrossRef]
48. Olimov, K.K.; Iqbal, A.; Masood, S. Systematic analysis of midrapidity transverse momentum spectra of identified charged particles in p+p collisions at $(s)^{1/2}$=2.76, 5.02, and 7 TeV at the LHC. *Int. J. Mod. Phys. A* **2020**, *35*, 2050167. [CrossRef]
49. Bíró, G.; Barnaföldi, G.G.; Biró, T.S.; Shen, K. Mass hierarchy and energy scaling of the Tsallis–Pareto parameters in hadron productions at RHIC and LHC energies. In *EPJ Web of Conferences*; EDP Sciences: Les Ulis, France, 2018; Volume 171, p. 14008.
50. Campanini, R. Quark Gluon Plasma and Multiplicity Dependence of Transverse Momentum in Hadronic Collisions. *Lett. Nuovo Cimento* **1985**, *44*, 343–350. [CrossRef]

51. Campanini, R. Possible Signals of new phenomena in hadronic interactions at $dn/d\eta = 5.5 \pm 1.2$. *arXiv* **2010**, arXiv:1012.5219.
52. Campanini, R.; Ferri, G. Experimental equation of state in proton-proton and proton-antiproton collisions and phase transition to quark gluon plasma. *Phys. Lett. B* **2011**, *703*, 237. [CrossRef]
53. ALICE Collab. Centrality Determination in Heavy Ion Collisions. ALICE-PUBLIC-2018-011. Available online: https://cds.cern.ch/record/2636623 (accessed on 1 December 2022).
54. Tsallis, C.; Mendes, R.; Plastino, A.R. The role of constraints within generalized nonextensive statistics. *Physica A* **1998**, *261*, 534–554. [CrossRef]
55. Biró, T.S.; Purcsel, G.; Ürmössy, K. Non-extensive approach to quark matter. *Eur. Phys. J. A* **2009**, *40*, 325–340. [CrossRef]